# Macromolecules

Article

RAFT Dispersion Alternating Copolymerization of Styrene with *N*-Phenylmaleimide: Morphology Control and Application as an Aqueous Foam Stabilizer

Pengcheng Yang, Oleksandr O. Mykhaylyk, Elizabeth R. Jones, and Steven P. Armes*

Department of Chemistry, University of Sheffield, Brook Hill, Sheffield, South Yorkshire S3 7HF, U.K.

S *Supporting Information*
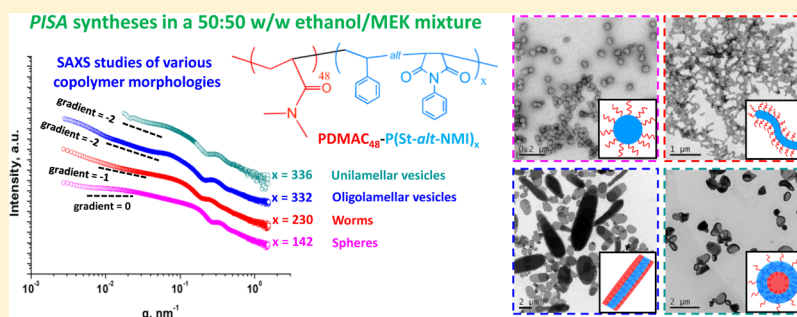
ABSTRACT: We report a new nonaqueous polymerization-induced self-assembly (PISA) formulation based on the reversible addition−fragmentation chain transfer (RAFT) dispersion alternating copolymerization of styrene with *N*-phenylmaleimide using a nonionic poly(*N*,*N*-dimethylacrylamide) stabilizer in a 50/50 w/w ethanol/methyl ethyl ketone (MEK) mixture. The MEK cosolvent is significantly less toxic than the 1,4-dioxane cosolvent reported previously [Yang, P.; et al. *Macromolecules* **2013**, *46*, 8545−8556]. The core-forming alternating copolymer block has a relatively high glass transition temperature (T_g), which leads to vesicular morphologies being observed during PISA, as well as the more typical sphere and worm phases. Each of these copolymer morphologies has been characterized by transmission electron microscopy (TEM) and small-angle X-ray scattering (SAXS) studies. TEM studies reveal micrometer-sized elliptical particles with internal structure, with SAXS analysis suggesting an oligolamellar vesicle morphology. This structure differs from that previously reported for a closely related PISA formulation utilizing a poly(methacrylic acid) stabilizer block for which unilamellar platelet-like particles are observed by TEM and SAXS. This suggests that interlamellar interactions are governed by the nature of the steric stabilizer layer. Moreover, using the MEK cosolvent also enables access to a unilamellar vesicular morphology, despite the high T_g of the alternating copolymer core-forming block. This was achieved by simply conducting the PISA synthesis at a higher temperature for a longer reaction time (80 °C for 24 h). Presumably, MEK solvates the core-forming block more than the previously utilized 1,4-dioxane cosolvent, which leads to greater chain mobility. Finally, preliminary experiments indicate that the worms are much more efficient stabilizers for aqueous foams than either the spheres or the oligolamellar elliptical vesicles.

INTRODUCTION

Over the past 5 years or so, polymerization-induced self-assembly (PISA) has become widely recognized as an efficient and versatile route to prepare block copolymer nano-objects.[1−26] In principle, PISA can be performed using any type of living polymerization chemistry, but in practice the majority of PISA literature examples are based on RAFT polymerization.[27−29] In PISA a soluble polymer A is chain-extended with a second polymer B that is insoluble in the solvent selected for the polymerization. Initially, polymer B grows in solution since it is solubilized by unreacted monomer B, but at a certain critical degree of polymerization (which can vary widely according to the precise PISA formulation), micellar nucleation occurs to produce AB diblock copolymer nanoparticles via microphase separation. Compared to traditional post-polymerization processing techniques, PISA enables diblock copolymer nanoparticles to be conveniently prepared in

a single step at high solids. Moreover, PISA is a generic approach that has been demonstrated for a wide range of solvents (e.g., water,[1−4,9,10,13] lower alcohols,[5−8,11,12,15,17] *n*-alkanes,[16,30,31] ionic liquids,[32] etc.).

In many cases the final sterically stabilized block copolymer nanoparticles have a well-defined spherical morphology, and the final particle diameter can be readily adjusted by targeting an appropriate degree of polymerization for the core-forming polymer B. However, if the stabilizer (polymer A) is relatively short, then under certain conditions alternative copolymer morphologies can be accessed, such as highly anisotropic worms or vesicles (a.k.a. polymersomes). In such cases an

evolution in copolymer morphology from spheres to worms to vesicles occurs during PISA.[33] This is driven by the gradual increase in the geometric packing parameter, P, which was originally introduced to explain surfactant self-assembly.[34]

Recently, we reported an unusual PISA formulation based on the RAFT alternating copolymerization of styrene with N-phenylmaleimide (NMI) using a poly(methacrylic acid)[35] stabilizer in an ethanol/1,4-dioxane solvent mixture. Originally, this system was designed to address the rather slow RAFT dispersion polymerization of styrene under PISA conditions, as reported by others.[5−8] However, we serendipitously found that the relatively high glass transition temperature (T_g) of the core-forming poly(styrene-alt-N-phenylmaleimide) P(St-alt-NMI) block prevented vesicle formation when targeting asymmetric diblock compositions. Instead, TEM studies confirmed that well-dispersed micrometer-sized block copolymer lamellae were formed with well-defined lamella thicknesses, but rather ill-defined sheet areas. In principle, such platelet-like particles offer an interesting wholly organic alternative to inorganic clay platelets.

In the present study, we revisit this RAFT alternating copolymerization system and modify the PISA formulation. More specifically, we replace the poly(methacrylic acid) (PMAA) stabilizer with a poly(N,N-dimethylacrylamide) (PDMAC) block, and the 1,4-dioxane cosolvent is replaced with a much less toxic alternative, methyl ethyl ketone (MEK). These two changes lead to some new features of interest, including subtle differences in the polymerization kinetics and the ability to access vesicle phase space. Furthermore, we utilize small-angle X-ray scattering (SAXS) to characterize the various block copolymer nano-objects. Finally, a potential application for such sterically stabilized nanoparticles in the area of foam stabilization is explored.

■ EXPERIMENTAL SECTION

Materials. All reagents were purchased from Sigma-Aldrich (UK) and were used as received, unless otherwise noted. 2,2′-Azobis-(isobutyronitrile) (AIBN, Molekular) was used as an initiator. N-Phenylmaleimide (NMI, 98%) was recrystallized from cyclohexane. Styrene (St, 99%) and N,N-dimethylacrylamide (99%) were each purified using column chromatography (basic alumina stationary phase) to remove inhibitor and then stored at −20 °C prior to use. Absolute ethanol (maximum water content = 0.1%) was supplied by VWR international S.A.S (Fontenay-sous-Bois, France). All other solvents were of HPLC quality and were supplied by Fisher Scientific (Loughborough, UK). All deuterated solvents were obtained from Goss Scientific (Cambridge, UK) and used as received. 4-Cyano-4-(2-phenylethanesulfanylthiocarbonyl)sulfanylpentanoic acid (PETTC) RAFT agent was prepared as described in the literature.[11]

Synthesis of Poly(N,N-dimethylacrylamide) (PDMAC) Chain Transfer Agent. In a 100 mL round-bottomed flask, PETTC (0.856 g, 2.52 mmol), AIBN (0.0414 g, 0.252 mmol; CTA/initiator molar ratio = 10), and N,N-dimethylacrylamide (DMAC; 15.0 g, 151 mmol) were dissolved in 1,4-dioxane (45.0 g) to obtain a 25% w/w DMAC solution. The reaction mixture was degassed using a dry nitrogen purge for 50 min at 0 °C before being placed into a preheated oil bath at 70 °C. After 2.5 h (81% DMAC conversion), the polymerization was quenched by cooling the reaction mixture to 20 °C and subsequently exposing it to air. 1,4-Dioxane (30 mL) was then added to dilute the solution, and unreacted DMAC monomer was removed by precipitation into a 10-fold excess of diethyl ether. This purification protocol was repeated twice. A yellow solid was obtained after drying under vacuum (10.3 g, 69% yield; M_n = 5800; M_w/M_n = 1.10). ¹H NMR spectroscopy indicated a mean degree of polymerization of 48 for the purified PDMAC macro-CTA in d_4-methanol (calculated by comparing the integrated aromatic signals due to the PETTC chain

end at 7.1−7.4 ppm with those assigned to the acrylamide backbone at 1.0−2.0 ppm).

Synthesis of Poly(methacrylic acid) (PMAA) Chain Transfer Agent. 2-Cyano-2-propyldithiobenzoate (CPDB) RAFT agent (0.686 g, 3.10 mmol), AIBN (0.051 g, 0.310 mmol; CTA/initiator molar ratio = 10.0), and methacrylic acid (MAA; 20.0 g, 232 mmol) were dissolved in ethanol (20.0 g) in a 100 mL round-bottomed flask. The reaction mixture was degassed using a dry nitrogen purge for 40 min at 0 °C before being placed into a preheated oil bath at 60 °C. After 12.5 h (54% MAA conversion), the polymerization was quenched by cooling the reaction mixture to 20 °C and subsequently exposing it to air. Ethanol (50 mL) was then added to dilute the solution, and unreacted MAA monomer was removed by precipitation into a 10-fold excess of diethyl ether. This purification protocol was repeated a further four times. A pink solid was obtained after drying under vacuum (8.2 g, 41% yield). ¹H NMR spectroscopy studies in d_4-methanol indicated a mean degree of polymerization of 84 for the PMAA macro-CTA (calculated by comparing the integrated signals assigned to the aromatic protons at 7.2−8.0 ppm with those due to the methacrylic polymer backbone at 0.4−2.5 ppm). After exhaustive methylation using excess trimethylsilyldiazomethane, THF GPC analysis (calibration with ten near-monodisperse poly(methyl methacrylate) standards) indicated an M_n of 8900 g mol⁻¹ and an M_w/M_n of 1.23.

RAFT Dispersion Alternating Copolymerization of Styrene with N-Phenylmaleimide Using a PDMAC₄₈ Macro-CTA in a 50/50 w/w Ethanol/MEK Mixture. In a typical formulation targeting PDMAC₄₈−P(St-alt-NMI)₃₅₀ at 20% w/w solids, PDMAC₄₈ macro-CTA (58.3 mg, 0.0114 mmol), AIBN (0.188 mg, 0.00114 mmol; CTA/initiator molar ratio = 10), styrene (208 mg, 2.00 mmol), and N-phenylmaleimide (346 mg, 2.00 mmol) were dissolved in a 50/50 w/w ethanol/MEK mixture (2.38 g). This reaction mixture was sealed in a 10 mL Schlenk flask and purged with nitrogen for 15 min at 20 °C, before being placed into a preheated oil bath at 70 °C. The RAFT alternating copolymerization was allowed to proceed for 5 h to ensure at least 90% total comonomer conversion and then quenched by exposure to air. Other block copolymer compositions were targeted by adjusting the relative molar concentrations of the PDMAC₄₈ macro-CTA and the styrene/N-phenylmaleimide comonomer mixture.

Synthesis of Poly(methacrylic acid)₈₄−Poly(styrene-alt-N-phenylmaleimide)$_x$ (PMAA₈₄−P(St-alt-NMI)$_x$) Diblock Copolymer Nanoparticles via RAFT Dispersion Alternating Copolymerization for Small-Angle X-ray Scattering (SAXS) Studies. These diblock copolymer nanoparticles were prepared as described in our previous paper.[35] The phase diagram reported for PMAA₇₉−P(St-alt-NMI)$_x$ diblock copolymer nano-objects in this prior study was used as an approximate guideline for targeting pure spheres, worms, and lamellae (x = 220, 420, and 700, respectively). Briefly, in a typical formulation targeting PMAA₈₄−P(St-alt-NMI)₂₂₀ spheres at 20% w/w solids, PMAA₈₄ macro-CTA (27.1 mg, 0.036 mmol), AIBN (0.119 mg, 0.00727 mmol; CTA/initiator molar ratio = 5.0), styrene (416 mg, 4.00 mmol), and N-phenylmaleimide (692 mg, 4.00 mmol) were dissolved in a 50/50 w/w ethanol/1,4-dioxane mixture (5.52 g). This reaction mixture was sealed in a small Schlenk flask (10 mL) and purged with dry nitrogen for 15 min at 20 °C, before being placed into a preheated oil bath at 70 °C. The RAFT alternating copolymerization was allowed to proceed for 10 h to ensure at least 90% comonomer conversion and then quenched by exposure to air. For GPC characterization, the MAA groups of the PMAA₈₄−P(St-alt-NMI)$_x$ diblock copolymers were fully esterified using excess trimethylsilyldiazomethane. Analyses were performed using a refractive index detector with HPLC-grade THF as eluent containing 2.0% v/v triethylamine at a flow rate of 1.0 mL min⁻¹ using a GPC column temperature of 30 °C. A series of ten near-monodisperse polystyrene standards (M_p = 162 to 371 100 g mol⁻¹) was used for calibration. Copolymer morphologies were confirmed via post-mortem TEM analysis (see Table S1 and Figure S1 in the Supporting Information).

Foam Preparation and Characterization. Selected PDMAC₄₈−P(St-alt-NMI)$_x$ diblock copolymer nanoparticles were evaluated as putative foam stabilizers. Foams were prepared by homogenizing 4.0

Scheme 1. RAFT Synthesis of Poly(N,N-dimethylacrylamide)$_{48}$ (PDMAC$_{48}$) Macro-CTA via Solution Polymerization in 1,4-Dioxane at 70 °C, Followed by RAFT Dispersion Alternating Copolymerization of Styrene (St) with N-Phenylmaleimide (NMI) in a 50/50 w/w Ethanol/MEK Mixture
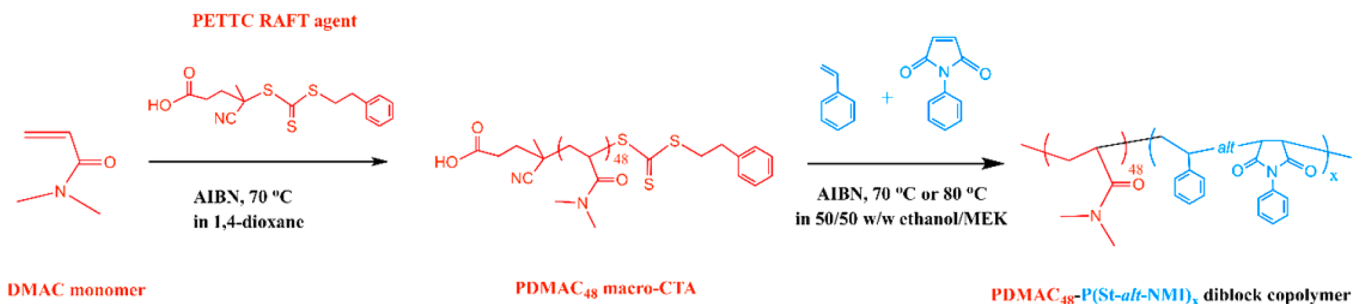
mL of 0.01−1.0% w/w aqueous copolymer dispersions using an IKA Ultra-Turrax T-18 homogenizer operating at 20 000 rpm for 1 min at 20 °C. The "foamability" was assessed by measuring the height of the foam layer, both immediately after homogenization and also after allowing the foams to settle for approximately 30 min at 20 °C. To assess foam stability, selected aqueous foams were stored at 20 °C, and foam heights were monitored over time. The foam structure was examined using a Motic DMBA300 digital biological microscope equipped with a built-in camera. Scanning electron microscopy (SEM) studies were conducted on dried samples mounted onto adhesive carbon disks with *no* further coating using a high-resolution field emission FEI Nova NonoSEM 450, operating at a relatively low voltage of 2 kV.

Copolymer Characterization. *^{1}H NMR Spectroscopy.* All ^{1}H NMR spectra were either recorded in d_4-methanol or d_6-DMSO using a 400 MHz Bruker Avance-400 spectrometer. Typically 64 scans were averaged per spectrum.

Gel Permeation Chromatography (GPC). Analyses were performed using an Agilent 1260 Infinity setup fitted with two PL gel 5 μm Mixed-C columns and one Phenogel 5 μm linear/mixed guard maintained at 60 °C. The DMF eluent contained 10 mM LiBr, and the flow rate was 1.0 mL min^{-1}. Calibration was achieved using a series of ten near-monodisperse poly(methyl methacrylate) (PMMA) standards ($M_p = 625−618\,000$ g mol^{-1}).

Dynamic Light Scattering (DLS). Hydrodynamic diameters were measured at 20 °C using a Malvern Zetasizer NanoZS Instrument equipped with a 4 mW He−Ne solid-state laser operating at 633 nm. Backscattered light was detected at 173°, and the mean particle diameter was calculated from the quadratic fitting of the correlation function over 30 runs each of 10 s duration. All measurements were performed in triplicate on 0.01% w/v copolymer dispersions in water.

Laser Diffraction. The diblock copolymer lamellae were also sized using a Malvern Mastersizer 2000 instrument equipped with a small volume Hydro 2000SM sample dispersion unit (ca. 50 mL), a He−Ne laser operating at 633 nm, and a solid-state blue laser operating at 466 nm. The stirring rate was adjusted to 1000 rpm.

Differential Scanning Calorimeter (DSC). The glass transition temperature was determined using a PerkinElmer Pyris 1 DSC instrument operating under a nitrogen atmosphere over a temperature range from 0 to 280 °C at a rate of 20 °C min^{-1}. The dried sample was hermetically sealed within an aluminum pan. Nitrogen was purged through the sample compartment at a flow rate of 30 mL min^{-1}, and the instrument was calibrated for heat flow and temperature using both indium and zinc standards.

Transmission Electron Microscopy (TEM). Copper/palladium TEM grids (Agar Scientific, UK) were surface-coated to yield a thin film of amorphous carbon. These grids were then plasma glow-discharged for 30 s to create a hydrophilic surface. A small volume (11 μL) of a dilute copolymer solution in ethanol was placed onto the freshly prepared grids for 60 s and then carefully blotted with filter paper to remove excess solution. To stain the nanoparticles, a 0.75% w/v uranyl formate solution (9 μL) was placed via micropipet onto the sample-loaded grid for 20 s and then carefully blotted to remove excess stain. The grids

were then dried using a vacuum hose. Imaging was performed using a FEI Tecnai Spirit instrument at 80 kV equipped with a Gatan 1k CCD camera.

Small-Angle X-ray Scattering. SAXS patterns were recorded either at a synchrotron source (ESRF, station ID02, Grenoble, France) or using a laboratory SAXS instrument (Xeuss 2.0, Xenocs, France) equipped with a liquid gallium MetalJet X-ray source (Excillum, Sweden). A monochromatic X-ray radiation (wavelength $\lambda = 0.0995$ or 0.134 nm) and 2D detector (Rayonix MX-170HS CCD or Dectris Pilatus 1M pixel detector) were used for these experiments. The SAXS cameras used for the measurements covered the q range from 0.004 to 2.0 nm^{-1} or 0.02 to 2.0 nm^{-1}, respectively, where $q = (4\pi \sin \theta)/\lambda$ is the modulus of the scattering vector and θ is half of the scattering angle. A vitrified quartz capillary flow-through cell of about 2 mm diameter was used as a sample holder for all measurements. X-ray scattering data were integrated and normalized using standard routines, software packages, and protocols available at synchrotron beamline ID02 or software package Foxtrot for the laboratory SAXS instrument. Irena SAS macros[36] for Igor Pro were utilized for background subtraction and further analysis. For SAXS measurements, the concentration of diblock copolymer nanoparticles was diluted from 20% w/w solids (i.e., as-synthesized) to 1.0% w/w solids using absolute ethanol. Most of the SAXS data presented in this work were obtained at the ESRF synchrotron source, unless otherwise stated.

■ RESULTS AND DISCUSSION

Synthesis of PDMAC$_{48}$−P(St-*alt*-NMI)$_x$ Diblock Copolymers via RAFT Dispersion Alternating Copolymerization. Scheme 1 outlines the general synthetic strategy for (i) the RAFT solution polymerization of DMAC and (ii) chain extension of this PDMAC macro-CTA via RAFT dispersion alternating copolymerization at 70 °C.

In principle, both dithioesters (e.g., benzyl dithiobenzoate) and trithiocarbonates are suitable chain transfer agents for both the RAFT homopolymerization of DMAC[37] and the subsequent alternating copolymerization.[38,39] However, in practice, the RAFT solution polymerization of DMAC using benzyl dithiobenzoate proved to be strongly retarded, with only 42% conversion being achieved after 24 h at 70 °C (target PDMAC DP = 60; [CTA]/[AIBN] molar ratio = 10). According to Feldermann and co-workers, this problem can be attributed to the relatively stable intermediate radical for such dithioester-mediated polymerizations.[40] Thus, a trithiocarbonate RAFT agent (i.e., 4-cyano-4-(2-phenylethanesulfanyl-thiocarbonyl)sulfanylpentanoic acid, PETTC) was selected to prepare the PDMAC macro-CTA using an AIBN initiator in 1,4-dioxane at 70 °C. This polymerization exhibited essentially no inhibition and proceeded relatively quickly, with almost complete monomer conversion being achieved within 3.5 h.[41] A large batch of PDMAC macro-CTA was prepared using this

Table 1. Summary of Monomer Conversions, GPC Molecular Weight Data, Particle Diameters, and TEM Morphologies Obtained for a Series of PDMAC$_{48}$−P(St-alt-NMI)$_x$ Diblock Copolymers Synthesized via RAFT Dispersion Alternating Copolymerization at Either 70 or 80 °C Using AIBN Initiator in a 50/50 w/w Ethanol/MEK Mixture at 20% w/w Solids[a]

entry no.	reaction time (h)	target DP for core-forming P(St-alt-NMI) block	overall comonomer conv[b] (%)	actual DP for core-forming P(St-alt-NMI) block[c]	GPC data		DLS data[d]		TEM morphology assignt[e]
					M_n	M_w/M_n	diameter (nm)	PDI	
1	5	150	95	142	29 200	1.36	58	0.08	S, SW
2	5	200	92	184	36 300	1.46	83	0.13	S, W
3	5	250	92	230	42 100	1.52	286	0.26	W
4	5	300	95	285	48 800	1.63	907	0.47	W, OLV
5	5	350	95	332	52 100	1.64	1388	0.31	OLV
6[f]	5	350	94	330	52 000	1.64	944	0.27	OLV, ULV
7[f]	24	350	96	336	52 300	1.66	664	0.13	ULV, OLV

[a]Conditions: [St]/[NMI] comonomer feed molar ratio = 1.0; [macro-CTA]/[AIBN] molar ratio = 10. [b]Determined by ^{1}H NMR spectroscopy in d_6-DMSO. [c]Actual DP of P(St-alt-NMI) = target DP of P(St-alt-NMI) × overall comonomer conversion. [d]Intensity-average DLS diameters were calculated using cumulants analysis software provided by the instrument manufacturer (Malvern, UK). PDI denotes the DLS polydispersity. [e]Abbreviations used in final column: S = spheres, SW = short worms (dimers, trimers), W = worms, OLV = oligolamellar vesicles, and ULV = unilamellar vesicles. [f]Polymerization was conducted at 80 °C.

protocol, and the polymerization was quenched after 2.5 h (81% conversion) in order to preserve high RAFT end-group fidelity. DMF GPC analysis confirmed that the resulting PDMAC macro-CTA had a narrow molecular weight distribution (M_w/M_n = 1.10; M_n = 5800 vs poly(methyl methacrylate) calibration standards), and a mean DP of 48 was determined by ^{1}H NMR spectroscopy (see Figure S2).

In our recent study, the RAFT dispersion alternating copolymerization of styrene with NMI was conducted using a poly(methacrylic acid) (PMAA) stabilizer in a 50/50 w/w ethanol/1,4-dioxane solvent mixture.[35] The 1,4-dioxane cosolvent was shown to be essential for this PISA formulation because it aids solubilization of NMI monomer within the growing diblock copolymer micelles. However, 1,4-dioxane has been classified as a probable human carcinogen.[42] Thus, it is not a desirable choice of solvent from an industrial prospective. Thus, a much less toxic solvent, methyl ethyl ketone (MEK), was identified as a suitable alternative to 1,4-dioxane for the present study. MEK is miscible with ethanol and is also a good solvent for the core-forming P(St-alt-NMI) block as well as both its constituent comonomers; it is also compatible with the PDMAC macro-CTA. (In contrast, MEK is incompatible with PMAA, which is the stabilizer block reported earlier for the RAFT dispersion alternating copolymerization of styrene with NMI.[35]) Table 1 summarizes the experimental data obtained for various chain extensions of the PDMAC$_{48}$ macro-CTA using a 1:1 mixture of styrene and NMI in 50/50 w/w ethanol/MEK. Each RAFT dispersion alternating copolymerization was relatively efficient, with final comonomer conversions exceeding 92% in all cases. However, molecular weight distributions were somewhat broader (M_w/M_n = 1.36−1.66) than those previously reported for PMAA-P(St-alt-NMI) diblock copolymers (i.e., M_w/M_n < 1.38).[35]

To further investigate this apparent reduction in control, a kinetic study was performed. GPC analysis indicated the presence of a low molecular weight shoulder corresponds to the unreacted PDMAC$_{48}$ macro-CTA at an early stage of the polymerization. This feature became less prominent during the alternating copolymerization and was barely discernible at 91% conversion (see Figure 1a and Figure S3 in the Supporting Information). This suggests that the initial activation of the PDMAC$_{48}$ macro-CTA proceeds at a similar rate to that of the alternating copolymerization. In contrast, a self-blocking
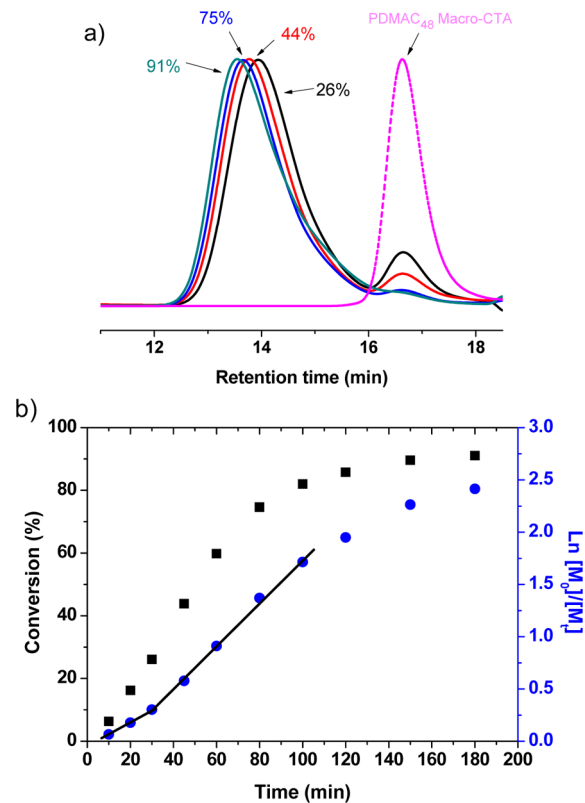

Figure 1. (a) Selected DMF GPC curves (refractive index detector) obtained for the RAFT dispersion alternating copolymerization of styrene with N-phenylmaleimide using a PDMAC$_{48}$ macro-CTA in a 50/50 w/w ethanol/MEK mixture at 70 °C when targeting a PMAA$_{48}$-P(St-alt-NMI)$_{350}$ diblock copolymer. (b) Comonomer conversion vs time curve (black squares) and corresponding semilogarithmic plot (blue circles) for the same RAFT dispersion alternating copolymerization. Conditions: [St]/[NMI] feed molar ratio = 1.0; [macro-CTA]/[AIBN] molar ratio = 10.0; copolymer concentration = 20% w/w solids.

experiment performed using the PDMAC$_{48}$ macro-CTA led to much cleaner chain extension for the RAFT solution polymerization of DMAC in 1,4-dioxane (see Figure S4). Using a UV GPC detector, the unreacted macro-CTA also exhibited a strong absorption at 300 nm due to its trithiocarbonate-based
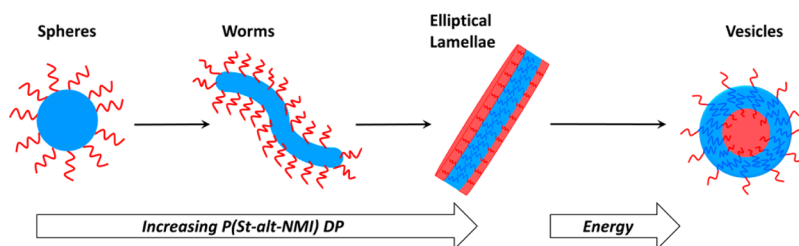
Figure 2. Schematic representation of the evolution in copolymer morphology for PDMAC$_{48}$–P(St-*alt*-NMI)$_x$ diblock copolymer nano-objects prepared via RAFT dispersion alternating copolymerization using polymerization-induced self-assembly (PISA).
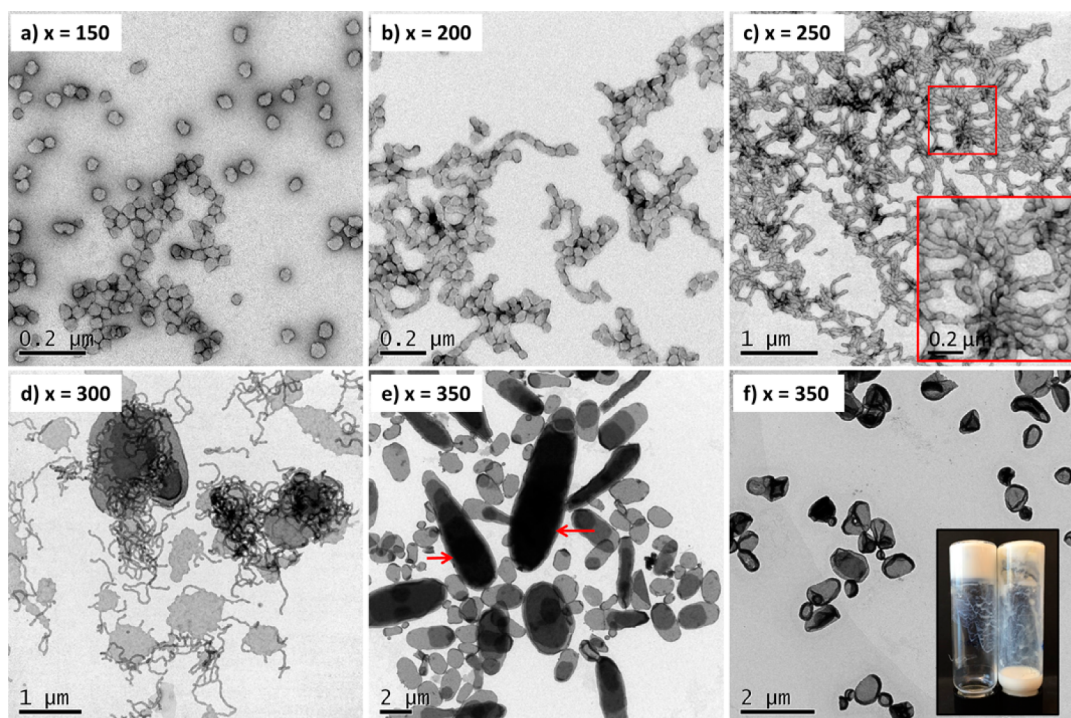

Figure 3. Representative TEM images illustrating (a–e) the evolution in copolymer morphology for PDMAC$_{48}$–P(St-*alt*-NMI)$_x$ diblock copolymer nano-objects prepared at 70 °C. (f) PDMAC$_{48}$–P(St-*alt*-NMI)$_{336}$ diblock copolymer vesicles (entry 7 in Table 1) synthesized at 80 °C using a 50/50 w/w ethanol/MEK mixture via RAFT dispersion alternating copolymerization at 20% w/w solids.

chain-end (see Figure S5). Hence, it appears that the low molecular weight shoulder discernible in Figure 1a is most likely the result of relatively slow macro-CTA consumption during polymerization, rather than loss of RAFT end-groups. As a result, some block copolymer chains are generated earlier than others, yielding a somewhat broader molecular weight distribution than that normally expected for a RAFT synthesis.[43] In related work, Charleux et al. reported relatively slow consumption of RAFT agent during chain extension of a PDMAC macro-CTA with *n*-butyl acrylate using a RAFT aqueous emulsion polymerization formulation.[44]

^{1}H NMR studies indicate that the rate of RAFT dispersion alternating copolymerization of styrene with NMI in a 50/50 w/w ethanol/MEK mixture using a PDMAC$_{48}$ macro-CTA is relatively fast at 70 °C, with more than 90% comonomer conversion being achieved within 3 h (see Figure 1b). The corresponding semilogarithmic plot (see Figure 1b) indicates a discernible increase in the rate of polymerization after 30 min, which corresponds to the onset of micellar nucleation (as judged by the sudden increase in solution turbidity).

Such observations are quite typical for many PISA syntheses[12−14,33] but are in marked contrast to our observations

during the PISA synthesis of PMAA-P(St-*alt*-NMI) diblock copolymer nanoparticles in a 50/50 w/w ethanol/1,4-dioxane mixture.[35] In this earlier study, a slightly *retarded* rate of polymerization was observed after micellar nucleation. This was attributed to the partial exclusion of one comonomer from the nascent copolymer micelles. In the present study, the rate of alternating copolymerization is approximately twice as fast as that reported earlier.[35] This suggests that MEK offers a further important advantage over 1,4-dioxane in such formulations: using the former cosolvent enables a higher comonomer concentration to be achieved within the swollen micelles. This difference can be rationalized by considering Hansen solubility parameters. Using the method of van Krevelen,[45] the total Hansen solubility parameter, δ_t, for the core-forming P(St-*alt*-NMI) chains was calculated to be 18.6 MPa$^{1/2}$, while literature δ_t values for 1,4-dioxane and MEK are 20.5 and 19 MPa$^{1/2}$, respectively.[46] Polymer solubility is optimal when the solubility parameters for a given polymer/solvent pair are similar.[47] Thus, the growing P(St-*alt*-NMI) chains are expected to be more swollen in a 50/50 w/w ethanol/MEK mixture than in a 50/50 w/w ethanol/1,4-dioxane mixture. The observed faster rate of polymerization is most likely due to the higher solubility of the

NMI comonomer in MEK compared to that in 1,4-dioxane. This interpretation is consistent with the 5-fold rate enhancement reported for a RAFT aqueous dispersion polymerization formulation.[33] In this latter case, a weakly hydrophobic poly(2-hydroxypropyl methacrylate) (PHPMA) core-forming block is well-solvated by unreacted HPMA monomer, leading to a relatively high local monomer concentration.

Characterization of Diblock Copolymer Morphologies. A series of $PDMAC_{48}$−$P(St$-alt-$NMI)_x$ diblock copolymers were prepared at 20% w/w solids in 50/50 w/w ethanol/MEK at 70 °C by systematically varying the target DP for the core-forming block from 150 to 350 (see Table 1). The *post mortem* copolymer morphologies were examined using DLS and TEM. As expected, the copolymer morphology proved to be sensitive to the DP of core-forming block (see Figure 2).

More specifically, TEM analysis confirmed that an approximately spherical morphology was produced when targeting a $P(St$-alt-$NMI)$ DP of 150 (see Figure 3a). DLS studies indicated an intensive-average hydrodynamic diameter of 58 nm, which is consistent with the number-average diameter estimated from TEM images. Increasing the target DP of the core-forming block up to 200 led to the production of slightly larger particles of 83 nm as judged by DLS, while TEM studies indicated that the copolymer morphology switched from spheres to short worms (see Figure 3b). The mean width of these copolymer worms is comparable to the mean diameter of the initial spheres, but the mean worm length is of the order of 100−200 nm. This suggests that these worms are formed via random 1D fusion of multiple spheres during PISA. Indeed, close inspection suggests that only partial coalescence of the original spheres occurs during PISA. At a target DP of 250, longer worms are obtained as judged by both TEM (see Figure 3c) and DLS studies (the "sphere-equivalent" diameter increases to 286 nm). Moreover, some degree of worm branching is also discernible for this $PDMAC_{48}$−$P(St$-alt-$NMI)_{250}$ copolymer (see Figure 3c, inset). This sphere-to-worm transition is the result of an increase in the volume of the core-forming chains during PISA.[34,48] Since the stabilizer block DP is fixed, the packing parameter for the growing diblock copolymer chains gradually increases as the alternating copolymerization progresses. As the copolymer becomes more asymmetric, the worm phase is favored over the initial sphere phase because this reduces the entropy penalty associated with chain stretching. When the evolution in copolymer morphology is under thermodynamic control, it is expected that worms can be transformed into vesicles during PISA provided that a sufficiently high DP for the $P(St$-alt-$NMI)$ core-forming block is targeted.[8,10,11,33] However, elliptical lamellae were obtained for $PDMAC_{48}$−$P(St$-alt-$NMI)_{332}$ instead of vesicles (see Figure 3e and Figure S6). Inspecting these TEM images, these particles are relatively large and rather polydisperse, with a "sphere-equivalent" volume-average diameter of around 2.6 μm as determined by laser diffraction. This sizing technique actually indicates a bimodal size distribution (see Figure S7). The formation of a lamellar phase, rather than a vesicular morphology, was previously reported by us for $PMAA_{79}$-$P(St$-alt-$NMI)_{618}$ diblock copolymers prepared via PISA using a 50/50 w/w ethanol/1,4-dioxane mixture. DSC measurements indicated a T_g of 219 °C for the $P(St$-alt-$NMI)_{300}$ homopolymer.[35] The highly inflexible nature of the copolymer chains impedes the "wrap-up" required to form vesicles,[49] even in the presence of 1,4-dioxane cosolvent at the polymerization temperature of 70 °C. Thus,

a kinetically trapped lamellar morphology is observed instead. In the present study, DSC studies confirmed that $PDMAC_{48}$−$P(St$-alt-$NMI)_{332}$ has a comparable T_g of 208 °C (see Figure S8), so the formation of elliptical lamellae in a 50/50 w/w ethanol/MEK mixture again appears to be related to unusually high chain rigidity. It is also noteworthy that an interesting intermediate copolymer morphology comprising lamellae with worms extending from the edge (see Figure 3d) was obtained for a target core DP of 300. Such a "flattened jellyfish" structure appears to be directly analogous to the more 3D-like "jellyfish" observed by Armes and co-workers when investigating the worm-to-vesicle transition observed for more conventional PISA formulations.[13,33,50]

As discussed above, MEK is a better solvent for the $P(St$-alt-$NMI)$ block than 1,4-dioxane, hence using the former solvent enhances the chain mobility of the core-forming block. In principle, this greater degree of solvation may provide an opportunity for copolymer chains to adopt a vesicular morphology, rather than form kinetically trapped lamellar structures. In order to examine this possibility, a $PDMAC_{48}$−$P(St$-alt-$NMI)_{336}$ was targeted at a slightly higher temperature and longer reaction time (80 °C for 24 h) under otherwise identical conditions. The molecular weight of the resulting copolymer (see entry 7 in Table 1) was almost the same as that determined for the block copolymer lamellae prepared at 70 °C for 5 h (see entry 5 in Table 1). However, the 20% w/w copolymer nanoparticles formed a free-flowing milky dispersion, rather than a highly viscous white paste (see Figure 3f, inset). DLS studies indicate a significant reduction in mean particle diameter to 634 nm, and the formation of polydisperse vesicles was confirmed by TEM (see Figure 3f). This lamellar-to-vesicle transition highlights the importance of chain mobility for the core-forming block during PISA syntheses. The higher reaction temperature and longer reaction time also play important roles because the morphology transition from lamellae to vesicles is rather slow. For example, if the PISA synthesis conducted at 80 °C was only allowed to proceed for 5 h (see entry 6 in Table 1), then a mixed phase containing a minor fraction of vesicles is produced (see Figure S9).

Although $PDMAC_{48}$−$P(St$-alt-$NMI)_{332}$ and $PMAA_{84}$−$P(St$-alt-$NMI)_{672}$ nano-objects were obtained via RAFT dispersion alternating copolymerization under comparable conditions (see Scheme 1 and also Scheme S1), they are remarkably different in their physical appearance. According to our earlier TEM studies, $PMAA_{84}$−$P(St$-alt-$NMI)_{672}$ lamellae appear to be relatively flat platelets and rather irregular in shape.[35] Conversely, the $PDMAC_{48}$−$P(St$-alt-$NMI)_{332}$ nano-objects obtained in the present study are distinctly elliptical. Moreover, the significantly darker regions within the TEM images (see arrows in Figure 3e) suggest some internal structure (see SAXS studies below). As discussed earlier, one important difference between these two PISA formulations is the replacement of 1,4-dioxane with MEK. However, replacing the PMAA stabilizer block with the PDMAC block may also account for the subtle difference in copolymer morphology. This is because the nature of the stabilizer block dictates the interparticle interactions: a thick, highly solvated stabilizer layer should promote a higher degree of dispersion (weaker interparticle interactions).[51] In the present study, the mean DP of the two stabilizer blocks differ significantly. Thus, it is not possible to know whether the higher degree of dispersion observed when using the PMAA block is the result of a thicker stabilizer layer or a more solvated stabilizer layer (or both).
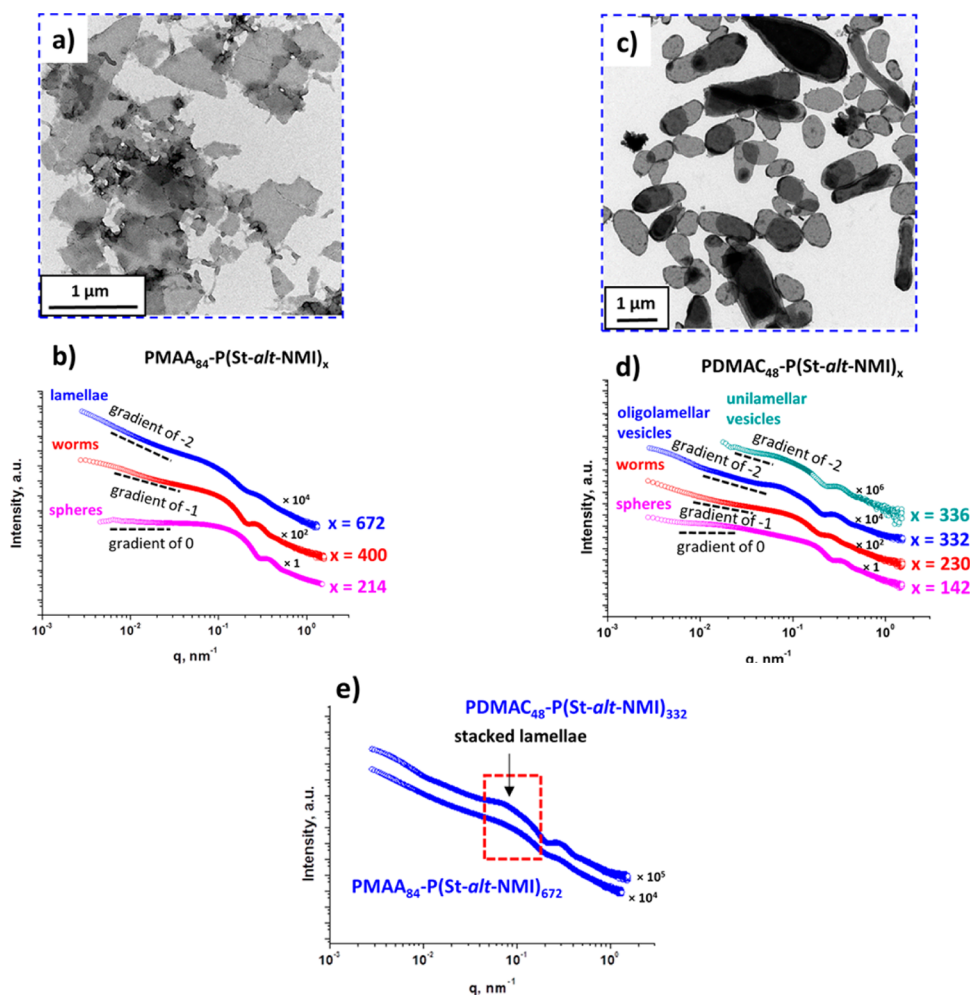
Figure 4. (a) Representative TEM image obtained for $PMAA_{84}$-$P(S\text{-}alt\text{-}NMI)_{672}$ lamellae. (b) $I(q)$ vs q plots obtained for the three pure $PMAA_{84}$–$P(S\text{-}alt\text{-}NMI)_x$ copolymer morphologies (where $x = 214$, 400, and 672 correspond to spheres, worms, and lamellae, respectively). (c) Representative TEM image obtained for $PDMAC_{48}$–$P(S\text{-}alt\text{-}NMI)_{332}$ elliptical oligolamellar vesicles. (d) $I(q)$ vs q plots obtained for the four pure $PDMAC_{48}$–$P(S\text{-}alt\text{-}NMI)_x$ copolymer morphologies (where $x = 142$, 230, 332, or 336 corresponds to spheres, worms, elliptical oligolamellar, or unilamellar vesicles, respectively) [N.B.: the unilamellar vesicles (green data set) were analyzed using a laboratory-based Xenocs/Excillum SAXS instrument]. (e) Comparison of $I(q)$ vs q plots obtained for $PMAA_{84}$–$P(S\text{-}alt\text{-}NMI)_{672}$ and $PDMAC_{48}$–$P(S\text{-}alt\text{-}NMI)_{332}$. The additional structure factor observed at $q \sim 0.07$ nm^{-1} indicates a relatively low degree of lamellar stacking (approximately 2−3 layers) in the latter case.

Small-Angle X-ray Scattering Studies of Diblock Copolymer Nano-Objects.

SAXS measurements on $PMAA_{84}$–$P(S\text{-}alt\text{-}NMI)_x$ and $PDMAC_{48}$–$P(S\text{-}alt\text{-}NMI)_x$ copolymer dispersions in ethanol are summarized in Figure 4 and Table 2. Scattering patterns obtained for a series of $PMAA_{84}$–$P(S\text{-}alt\text{-}NMI)_x$ nano-objects prepared when targeting progressively higher DPs ($x = 214$, 400, or 672) exhibit a gradual change in gradient at low q (0, −1, and −2, respectively; see Figure 4b and Table 2), indicating an evolution in copolymer morphology from spheres ($x = 214$) to worms ($x = 400$) to platelet-like lamellae ($x = 672$).[52] These observations are fully consistent with TEM studies reported previously.[35] Similar results were obtained for the series of $PDMAC_{48}$–$P(S\text{-}alt\text{-}NMI)_x$ dispersions: spheres were obtained for $x = 142$, worms for $x = 230$, and lamellar-like nano-objects for $x = 332$ (see Figure 4d and Table 2), which are in fairly good agreement with the corresponding TEM images (see Figures 3a, 3c, and 3e, respectively). However, closer inspection indicates that the scattering pattern for the spherical morphology actually shows a nonzero gradient at around $q \sim 0.1$ nm^{-1}, which only becomes a zero gradient at $q \sim 0.01$ nm^{-1}. This suggests that these

"spheres" also contain populations of dimers and trimers (see Figures 3a and 3b).[13] A subtle difference between the two scattering patterns recorded for the $PMAA_{84}$-$P(S\text{-}alt\text{-}NMI)_{400}$ and $PDMAC_{48}$–$P(S\text{-}alt\text{-}NMI)_{230}$ worm dispersions is also observed. The latter pattern (see Figure 4d) shows an upturn in X-ray intensity at very low q ($q < 0.008$ nm^{-1}). This suggests branched worms and/or an interconnected worm network akin to mass fractals,[53] as suggested by the TEM image shown in Figure 3c. The SAXS pattern corresponding to the $PDMAC_{48}$–$P(S\text{-}alt\text{-}NMI)_{332}$ lamellar-like nano-objects has a pronounced peak at $q \sim 0.07$ nm^{-1}. Rudimentary analysis using an existing SAXS model for a lamellar structure[54] suggests that this feature most likely corresponds to oligolamellar vesicles comprising two or three stacked lamellae (see Figure 4e). This is consistent with TEM images (see Figure 3e) that show stacked elliptical nano-objects as a result of collapsed oligolamellar vesicles. Similar oligolamellar vesicles have been recently reported for aqueous PISA formulations and characterized using SAXS and TEM.[13] Moreover, the mean vesicle membrane thickness estimated from SAXS (29.9 nm; see Table 2 and Figure 4d) is significantly smaller than the *period* of the stacks, d ($d = 2\pi/q =$

Table 2. Summary of SAXS Data Recorded for the Seven PMAA$_{84}$-P(St-*alt*-NMI)$_x$ (x = 214, 400, or 672) and PDMAC$_{48}$−P(St-*alt*-NMI)$_x$ (x = 142, 230, 332, or 336) Diblock Copolymer Nano-Objects Recorded as 1.0% w/w Dispersions in Absolute Ethanol^a

diblock copolymer composition	gradient at low q	copolymer morphology	q_{min} (nm^{-1})	dimensions^b (nm)
PMAA$_{84}$−P(St-*alt*-NMI)$_{214}$	0	spheres	0.29	R_{sp} = 15.5
PMAA$_{84}$−P(St-*alt*-NMI)$_{400}$	−1	worms	0.21	R_w = 18.2
PMAA$_{84}$−P(St-*alt*-NMI)$_{672}$	−2	lamellae	0.20	L = 31.4
PDMAC$_{48}$−P(St-*alt*-NMI)$_{142}$	0	spheres, short worms	0.27	R_{sp} = 16.6
PDMAC$_{48}$−P(St-*alt*-NMI)$_{230}$	−1	worms	0.20	R_w = 19.1
PDMAC$_{48}$−P(St-*alt*-NMI)$_{332}$	−2	oligolamellar vesicles	0.21	L = 29.9
PDMAC$_{48}$−P(St-*alt*-NMI)$_{336}$	−2	unilamellar vesicles	0.21	L = 29.9

^{a}The gradient at low q indicates the copolymer morphology, while the position of the first minimum (q_{min}) indicates the nano-object dimensions (sphere radius, R_{sp}, worm radius, R_w, and lamellae or vesicle membrane thickness, L). ^{b}Characteristic dimensions for each copolymer morphology can be calculated from the position of the first intensity minimum, q_{min}, in the scattering patterns (Figures 5d and 5e) using the expressions $q_{min}R_{sp}$ = 4.49, $q_{min}R_w$ = 3.83, and $q_{min}L$ = 2π,[52] where R_{sp} is the sphere radius, R_w is the worm radius, and L is the thickness of the lamellae or vesicle membrane.

$2\pi/0.07$ nm^{-1} ∼ 90 nm). This suggests that the individual lamellae are well-separated from each other, which is consistent with the micrometer-sized elliptical oligolamellar vesicles shown in Figure 3e. A slight modification of the synthetic protocol used for the oligolamellar vesicles involved conducting the alternating copolymerization at a slightly higher temperature and significantly longer reaction time (80 °C for 24 h). This produced a mainly unilamellar vesicle morphology, as judged by TEM analysis (see Figure 3f), and confirmed by SAXS studies (see Figure 4d and Table 2). Indeed, the q ∼ 0.07 nm^{-1} feature that characterizes an oligolamellar morphology is substantially attenuated, with only a very weak broad feature remaining at q ∼ 0.055 nm^{-1}. This suggests remnants of the oligolamellar structure, with a reduced number of stacked lamellae and a corresponding increase in the *period* for the stacks, d ($d = 2\pi/q = 2\pi/0.055$ nm^{-1} ∼ 115 nm).

The nano-object cross-section can be estimated from the position of the first minima observed in the corresponding SAXS pattern (Table 2, final column). This analysis suggests that lowering the mean DP of the core-forming P(St-*alt*-NMI) block by roughly a factor of 2 results in virtually the same cross-section dimensions (and similar copolymer morphologies) for the two series of nano-objects. Given that the PDMAC$_{48}$ and PMAA$_{84}$ stabilizer DPs also differ by a factor of approximately two, this suggests that each copolymer morphology corresponds to a characteristic stabilizer volume fraction, which is consistent with the well-known concept of a geometric packing parameter for block copolymer chains.[48]

Foam Stabilization Experiments. It is well-known that inorganic or organic particles of appropriate wettability can confer remarkable stabilization on air bubbles and foams.[55−60] In this context, we have described the use of near-monodisperse sterically stabilized polymer latexes as foam stabilizers, with the latex dimensions conferring interesting optical properties on the dried foams, e.g., Moiré effects, iridescence, or structural color.[61−63] Encouraged by our recent success in using block copolymer nano-objects to stabilize Pickering emulsions,[64−66] we decided to evaluate the new nanoparticles described in the present study as putative aqueous foam stabilizers.
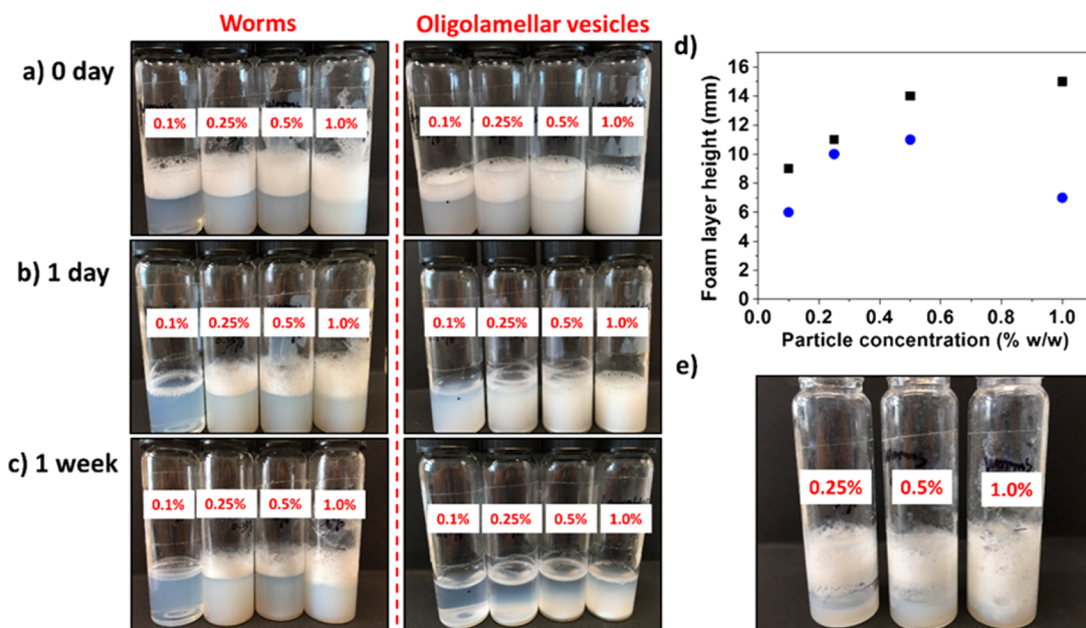

Figure 5. Digital images recorded for aqueous foams stabilized using PDMAC$_{48}$−P(St-*alt*-NMI)$_{230}$ worms and PDMAC$_{48}$−P(St-*alt*-NMI)$_{332}$ oligolamellar vesicles respectively: (a) 30 min after foam generation and then after storage at 20 °C for (b) 1 day and (c) 1 week. (d) Initial foam height (recorded 30 min after foam generation) as a function of copolymer concentration: the black and blue data sets correspond respectively to the worm-stabilized and oligolamellar vesicle-stabilized foams shown in (a). (e) Digital photographs recorded for PDMAC$_{48}$−P(St-*alt*-NMI)$_{230}$ worm-stabilized foams during slow evaporation of the underlying aqueous phase.
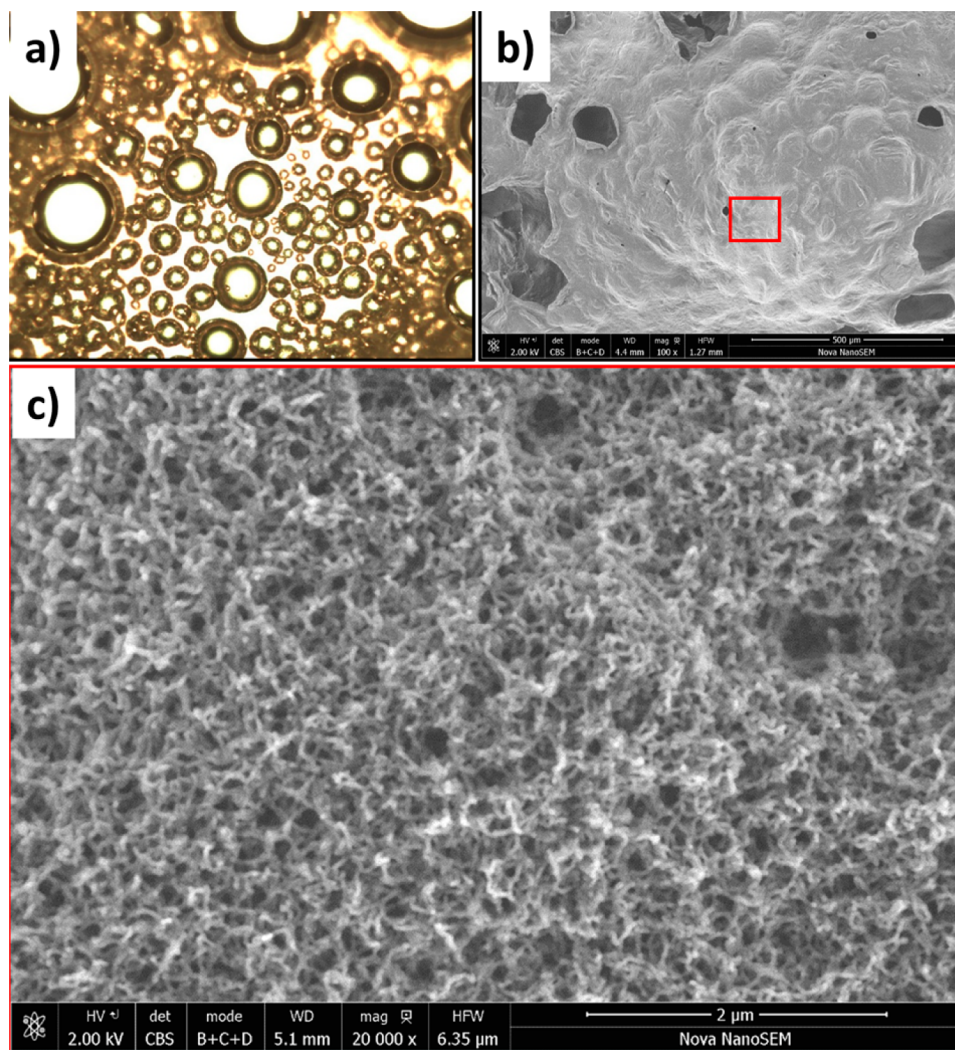
Figure 6. Optical micrograph (a) and SEM image (b) recorded for foams prepared using 1.0% w/w PDMAC$_{48}$−P(St-*alt*-NMI)$_{230}$ worms. (c) A dense layer of adsorbed worms is clearly discernible at the surface of the dried foam bubbles when examined by SEM at higher magnification.

In preliminary screening experiments, PDMAC$_{48}$−P(St-*alt*-NMI)$_x$ spheres, worms, and oligolamellar vesicles (see entries 1, 3, and 5 in Table 1) were evaluated in turn at a constant copolymer concentration of 0.50% w/w. However, the 58 nm PDMAC$_{48}$−P(St-*alt*-NMI)$_{142}$ spheres proved to be very inefficient foam stabilizers (see Figure S10). This suggests that these spheres are only weakly adsorbed at the air−water interface and so cannot prevent bubble coalescence.[67] In contrast, relatively stable foams were obtained using both worms and oligolamellar vesicles. The effect of varying the copolymer concentration from 0.1 to 1.0% w/w on foam formation was studied in more detail for these two systems (see Figure 5). Using PDMAC$_{48}$−P(St-*alt*-NMI)$_{230}$ worms, foams can be produced using just 0.1% w/w copolymer, with the foam layer height increasing with copolymer concentration (see Figure 5a). In principle, using higher copolymer concentrations should promote worm adsorption at the air−water interface, enabling a higher interfacial area to be stabilized. PDMAC$_{48}$−P(St-*alt*-NMI)$_{332}$ oligolamellar vesicles were also able to stabilize foams at all copolymer concentrations investigated, but these foam heights were always lower than the corresponding foams prepared using the worms (see Figure 5d). In addition, the maximum foam height was obtained at

0.50% w/w rather than 1.0% w/w copolymer, which may indicate saturation coverage at the air−water interface. More importantly, the oligolamellar vesicle-stabilized foams had more or less coalesced on standing at 20 °C within 24 h (see Figure 5b). In contrast, worm-stabilized foams remained largely intact under the same conditions when prepared at copolymer concentrations above 0.1% w/w (but a foam prepared using 0.1% w/w worms completely collapsed within 24 h on standing at 20 °C). Remarkably, these worm-stabilized foams maintained their 3D structure even after the underlying liquid had slowly evaporated through the foam layer (see Figure 5e).

Optical micrographs recorded for 50−300 μm air bubbles stabilized using 1.0% w/w PDMAC$_{48}$−P(St-*alt*-NMI)$_{230}$ worms are shown in Figure 6a. Stable bubbles require (i) strong particle adsorption at the air−water interface and (ii) high surface coverage. This leads to the formation of so-called "armored" bubbles; thus, normal coalescence mechanisms via gas diffusion and liquid drainage can be arrested.[55−60] Because of the highly anisotropic nature of the PDMAC$_{48}$−P(St-*alt*-NMI)$_{230}$ worms, they adsorb much more strongly at an interface than the corresponding precursor spheres.[65] Furthermore, recent studies suggest that the hydrophobic air−water interface also exhibits anionic character.[68,69] Hence, the

nonionic character of the stabilizer block enables efficient adsorption of PDMAC$_{48}$−P(St-*alt*-NMI)$_{230}$ worms at the air−water interface. In contrast, a control experiment conducted at pH 7 using PMAA$_{84}$−P(St-*alt*-NMI)$_{400}$ worms produced no stable aqueous foam at all (see Figure S10). Presumably, this is the result of the anionic particle surface charge conferred by the ionized PMAA stabilizer chains, which prevents adsorption at the anionic air−water interface due to an unfavorable electrostatic interaction.[70] SEM images recorded for 1.0% w/w PDMAC$_{48}$−P(St-*alt*-NMI)$_{230}$ worm foams after drying at 25 °C are shown in Figures 6b and 6c. Individual polydisperse bubbles are discernible at low magnification, and their dimensions are consistent with those observed for the wet foam by optical microscopy. Inspecting the upper surface of the dried foams confirmed that the air bubble surface comprised a highly entangled mesh of overlapping worms. The long-term foam stability therefore arises from steric repulsion between these dense layers of adsorbed worms, which suppress gas diffusion and prevent coalescence via rupture of the liquid film between adjacent bubbles during liquid drainage.[55] Moreover, the relatively rigid nature of the individual worms most likely leads to greater mechanical integrity of the adsorbed worm layer, which further enhances the foam stability.[55]

CONCLUSIONS

A new PISA formulation based on the RAFT dispersion alternating copolymerization of styrene with *N*-phenylmaleimide is reported that utilizes a 50/50 w/w ethanol/MEK mixture and a nonionic poly(*N,N*-dimethylacrylamide) stabilizer. The MEK cosolvent is significantly less toxic than the 1,4-dioxane cosolvent reported previously.[35] The core-forming alternating copolymer block has a relatively high T_g, which leads to bilayer structures being observed during PISA as well as the more typical sphere and worm phases. More specifically, TEM studies indicate the formation of micrometer-sized oligolamellar elliptical vesicles, with SAXS analysis suggesting a mean degree of lamellae stacking of 2−3 layers. This copolymer morphology differs from that previously reported for a closely related PISA formulation utilizing a poly-(methacrylic acid) stabilizer block and 1,4-dioxane cosolvent, for which unilamellar platelets were observed by TEM[35] (with this prior structural assignment being corroborated by SAXS in the present work). This suggests that interlamellar interactions are governed by the nature and thickness of the steric stabilizer layer. Moreover, using the MEK cosolvent also enables access to an almost pure unilamellar vesicle morphology. This morphology was accessed by simply conducting the PISA synthesis at a higher temperature for a longer reaction time (80 °C for 24 h). Finally, preliminary experiments indicate that the worms are much more efficient stabilizers for aqueous foams than either the spheres or the oligolamellar vesicles.

ASSOCIATED CONTENT

(S) Supporting Information

The Supporting Information is available free of charge on the ACS Publications website at DOI: 10.1021/acs.macromol.6b01563.

Synthesis and characterization data for the PMAA$_{84}$−P(St-*alt*-NMI)$_x$ diblock copolymers used for the SAXS studies; ^{1}H NMR spectrum of PDMAC$_{48}$ macro-CTA; DMF GPC curves obtained for PDMAC$_{48}$ macro-CTA self-blocking chain extension experiment; additional

DMF GPC curves obtained for PDMAC$_{48}$ macro-CTA and various PDMAC$_{48}$−P(St-*alt*-NMI)$_x$ diblock copolymers; volume-average particle size distribution, a DSC curve and additional TEM images obtained for PDMAC$_{48}$−P(St-*alt*-NMI)$_{332}$ oligolamellar vesicles; digital photograph showing aqueous foams stabilized by various PDMAC$_{48}$−P(St-*alt*-NMI)$_x$ nano-objects; control experiment conducted using anionic PMAA$_{84}$−P(St-*alt*-NMI)$_{400}$ worms (PDF)

AUTHOR INFORMATION

Corresponding Author
*E-mail s.p.armes@sheffield.ac.uk (S.P.A.).

Present Address
P.Y.: Nuplex Resins Ltd., North Woolwich Road, Silvertown, London E16 2AF, UK.

Notes
The authors declare no competing financial interest.

REFERENCES

(1) Ferguson, C. J.; Hughes, R. J.; Nguyen, D.; Pham, B. T. T.; Gilbert, R. G.; Serelis, A. K.; Such, C. H.; Hawkett, B. S. Ab Initio Emulsion Polymerization by RAFT-Controlled Self-Assembly. *Macromolecules* 2005, 38, 2191−2204.

(2) Boisse, S.; Rieger, J.; Di-Cicco, A.; Albouy, P.-A.; Bui, C.; Li, M.-H.; Charleux, B. Synthesis via RAFT of Amphiphilic Block Copolymers with Liquid-Crystalline Hydrophobic Block and Their Self-Assembly in Water. *Macromolecules* 2009, 42, 8688−8696.

(3) Brusseau, S. g. n.; D'Agosto, F.; Magnet, S. p.; Couvreur, L.; Chamignon, C. c.; Charleux, B. Nitroxide-Mediated Copolymerization of Methacrylic Acid and Sodium 4-Styrenesulfonate in Water Solution and One-Pot Synthesis of Amphiphilic Block Copolymer Nano-particles. *Macromolecules* 2011, 44, 5590−5598.

(4) Zhang, W.; D'Agosto, F.; Boyron, O.; Rieger, J.; Charleux, B. Toward a Better Understanding of the Parameters that Lead to the Formation of Nonspherical Polystyrene Particles via RAFT-Mediated One-Pot Aqueous Emulsion Polymerization. *Macromolecules* 2012, 45, 4075−4084.

(5) Wan, W.-M.; Hong, C.-Y.; Pan, C.-Y. One-pot synthesis of nanomaterials via RAFT polymerization induced self-assembly and morphology transition. *Chem. Commun.* 2009, 5883−5885.

(6) Cai, W.-M.; Wan, W.-M.; Hong, C.-Y.; Huang, C.-Q.; Pan, C.-Y. Morphology transitions in RAFT polymerization. *Soft Matter* 2010, 6, 5554−5561.

(7) Wan, W.-M.; Pan, C.-Y. One-pot synthesis of polymeric nanomaterials via RAFT dispersion polymerization induced self-assembly and re-organization. *Polym. Chem.* 2010, 1, 1475−1484.

(8) He, W.-D.; Sun, X.-L.; Wan, W.-M.; Pan, C.-Y. Multiple Morphologies of PAA-b-PSt Assemblies throughout RAFT Dispersion Polymerization of Styrene with PAA Macro-CTA. *Macromolecules* **2011**, *44*, 3358−3365.

(9) Li, Y.; Armes, S. P. RAFT Synthesis of Sterically Stabilized Methacrylic Nanolatexes and Vesicles by Aqueous Dispersion Polymerization. *Angew. Chem., Int. Ed.* **2010**, *49*, 4042−4046.

(10) Sugihara, S.; Blanazs, A.; Armes, S. P.; Ryan, A. J.; Lewis, A. L. Aqueous Dispersion Polymerization: A New Paradigm for in Situ Block Copolymer Self-Assembly in Concentrated Solution. *J. Am. Chem. Soc.* **2011**, *133*, 15707−15713.

(11) Semsarilar, M.; Jones, E. R.; Blanazs, A.; Armes, S. P. Efficient Synthesis of Sterically-Stabilized Nano-Objects via RAFT Dispersion Polymerization of Benzyl Methacrylate in Alcoholic Media. *Adv. Mater.* **2012**, *24*, 3378−3382.

(12) Jones, E. R.; Semsarilar, M.; Blanazs, A.; Armes, S. P. Efficient Synthesis of Amine-Functional Diblock Copolymer Nanoparticles via RAFT Dispersion Polymerization of Benzyl Methacrylate in Alcoholic Media. *Macromolecules* **2012**, *45*, 5091−5098.

(13) Warren, N. J.; Mykhaylyk, O. O.; Mahmood, D.; Ryan, A. J.; Armes, S. P. RAFT Aqueous Dispersion Polymerization Yields Poly(ethylene glycol)-Based Diblock Copolymer Nano-Objects with Predictable Single Phase Morphologies. *J. Am. Chem. Soc.* **2013**, *136*, 1023−1033.

(14) Hanisch, A.; Yang, P.; Kulak, A. N.; Fielding, L. A.; Meldrum, F. C.; Armes, S. P. Phosphonic Acid-Functionalized Diblock Copolymer Nano-Objects via Polymerization-Induced Self-Assembly: Synthesis, Characterization, and Occlusion into Calcite Crystals. *Macromolecules* **2015**, *49*, 192−204.

(15) Pei, Y.; Lowe, A. B. Polymerization-induced self-assembly: ethanolic RAFT dispersion polymerization of 2-phenylethyl methacrylate. *Polym. Chem.* **2014**, *5*, 2342−2351.

(16) Pei, Y.; Noy, J.-M.; Roth, P. J.; Lowe, A. B. Soft Matter Nanoparticles with Reactive Coronal Pentafluorophenyl Methacrylate Residues via Non-Polar RAFT Dispersion Polymerization and Polymerization-Induced Self-Assembly. *J. Polym. Sci., Part A: Polym. Chem.* **2015**, *53*, 2326−2335.

(17) Garrett, E. T.; Pei, Y.; Lowe, A. B. Microwave-assisted synthesis of block copolymer nanoparticles via RAFT with polymerization-induced self-assembly in methanol. *Polym. Chem.* **2016**, *7*, 297−301.

(18) Tan, J.; Sun, H.; Yu, M.; Sumerlin, B. S.; Zhang, L. Photo-PISA: Shedding Light on Polymerization-Induced Self-Assembly. *ACS Macro Lett.* **2015**, *4*, 1249−1253.

(19) Zhao, W.; Gody, G.; Dong, S.; Zetterlund, P. B.; Perrier, S. Optimization of the RAFT polymerization conditions for the in situ formation of nano-objects via dispersion polymerization in alcoholic medium. *Polym. Chem.* **2014**, *5*, 6990−7003.

(20) Charleux, B.; Delaittre, G.; Rieger, J.; D'Agosto, F. Polymerization-Induced Self-Assembly: From Soluble Macromolecules to Block Copolymer Nano-Objects in One Step. *Macromolecules* **2012**, *45*, 6753−6765.

(21) Sun, J.-T.; Hong, C.-Y.; Pan, C.-Y. Formation of the block copolymer aggregates via polymerization-induced self-assembly and reorganization. *Soft Matter* **2012**, *8*, 7753−7767.

(22) Sun, J.-T.; Hong, C.-Y.; Pan, C.-Y. Recent advances in RAFT dispersion polymerization for preparation of block copolymer aggregates. *Polym. Chem.* **2013**, *4*, 873−881.

(23) Rieger, J. Guidelines for the Synthesis of Block Copolymer Particles of Various Morphologies by RAFT Dispersion Polymerization. *Macromol. Rapid Commun.* **2015**, *36*, 1458−1471.

(24) Warren, N. J.; Armes, S. P. Polymerization-Induced Self-Assembly of Block Copolymer Nano-objects via RAFT Aqueous Dispersion Polymerization. *J. Am. Chem. Soc.* **2014**, *136*, 10174−10185.

(25) Derry, M. J.; Fielding, L. A.; Armes, S. P. Polymerization-induced self-assembly of block copolymer nanoparticles via RAFT non-aqueous dispersion polymerization. *Prog. Polym. Sci.* **2016**, *52*, 1−18.

(26) Canning, S. L.; Smith, G. N.; Armes, S. P. A Critical Appraisal of RAFT-Mediated Polymerization-Induced Self-Assembly. *Macromolecules* **2016**, *49*, 1985−2001.

(27) Chiefari, J.; Chong, Y. K.; Ercole, F.; Krstina, J.; Jeffery, J.; Le, T. P. T.; Mayadunne, R. T. A.; Meijs, G. F.; Moad, C. L.; Moad, G.; Rizzardo, E.; Thang, S. H. Living Free-Radical Polymerization by Reversible Addition-Fragmentation Chain Transfer: The RAFT Process. *Macromolecules* **1998**, *31*, 5559−5562.

(28) Moad, G.; Rizzardo, E.; Thang, S. H. Living Radical Polymerization by the RAFT Process. *Aust. J. Chem.* **2005**, *58*, 379−410.

(29) Moad, G.; Rizzardo, E.; Thang, S. H. Living Radical Polymerization by the RAFT Process − A Second Update. *Aust. J. Chem.* **2009**, *62*, 1402−1472.

(30) Fielding, L. A.; Derry, M. J.; Ladmiral, V.; Rosselgong, J.; Rodrigues, A. M.; Ratcliffe, L. P. D.; Sugihara, S.; Armes, S. P. RAFT dispersion polymerization in non-polar solvents: facile production of block copolymer spheres, worms and vesicles in n-alkanes. *Chemical Science* **2013**, *4*, 2081−2087.

(31) Lopez-Oliva, A. P.; Warren, N. J.; Rajkumar, A.; Mykhaylyk, O. O.; Derry, M. J.; Doncom, K. E. B.; Rymaruk, M. J.; Armes, S. P. Polydimethylsiloxane-Based Diblock Copolymer Nano-objects Prepared in Nonpolar Media via RAFT-Mediated Polymerization-Induced Self-Assembly. *Macromolecules* **2015**, *48*, 3547−3555.

(32) Dong, S.; Zhao, W.; Lucien, F. P.; Perrier, S.; Zetterlund, P. B. Polymerization induced self-assembly: tuning of nano-object morphology by use of CO_2. *Polym. Chem.* **2015**, *6*, 2249−2254.

(33) Blanazs, A.; Madsen, J.; Battaglia, G.; Ryan, A. J.; Armes, S. P. Mechanistic Insights for Block Copolymer Morphologies: How Do Worms Form Vesicles? *J. Am. Chem. Soc.* **2011**, *133*, 16581−16587.

(34) Israelachvili, J. In *Intermolecular & Surface Forces*, 2nd ed.; Academic Press: London, 1991.

(35) Yang, P.; Ratcliffe, L. P. D.; Armes, S. P. Efficient Synthesis of Poly(methacrylic acid)-*block*-Poly(styrene-alt-N-phenylmaleimide) Diblock Copolymer Lamellae Using RAFT Dispersion Polymerization. *Macromolecules* **2013**, *46*, 8545−8556.

(36) Ilavsky, J.; Jemian, P. R. Irena: tool suite for modeling and analysis of small-angle scattering. *J. Appl. Crystallogr.* **2009**, *42*, 347−353.

(37) Barner-Kowollik, C.; Davis, T. P.; Heuts, J. P. A.; Stenzel, M. H.; Vana, P.; Whittaker, M. RAFTing Down Under: Tales of Missing Radicals, Fancy, Architectures, and Mysterious Holes.pdf. *J. Polym. Sci., Part A: Polym. Chem.* **2003**, *41*, 365−375.

(38) Li, A.; Lu, J. Controlled/living RAFT polymerization of N-phenyl maleimide and synthesis of its block copolymers. *J. Appl. Polym. Sci.* **2009**, *114*, 2469−2473.

(39) Ma, J.; Cheng, C.; Sun, G.; Wooley, K. L. Well-Defined Polymers Bearing Pendent Alkene Functionalities via Selective RAFT Polymerization. *Macromolecules* **2008**, *41*, 9080−9089.

(40) Feldermann, A.; Coote, M. L.; Stenzel, M. H.; Davis, T. P.; Barner-Kowollik, C. Consistent Experimental and Theoretical Evidence for Long-Lived Intermediate Radicals in Living Free Radical Polymerization. *J. Am. Chem. Soc.* **2004**, *126*, 15915−15923.

(41) Rieger, J.; Grazon, C.; Charleux, B.; Alaimo, D.; Jerome, C. Pegylated thermally responsive block copolymer micelles and nanogels via in situ RAFT aqueous dispersion polymerization. *J. Polym. Sci., Part A: Polym. Chem.* **2009**, *47*, 2373−2390.

(42) Kociba, R. J.; McCollister, S. B.; Park, C.; Torkelson, T. R.; Gehring, P. J. 1,4-Dioxane. I. Results of a 2-year ingestion study in rats. *Toxicol. Appl. Pharmacol.* **1974**, *30*, 275−286.

(43) Wong, K. H.; Davis, T. P.; Barner-Kowollik, C.; Stenzel, M. H. Honeycomb structured porous films from amphiphilic block copolymers prepared via RAFT polymerization. *Polymer* **2007**, *48*, 4950−4965.

(44) Rieger, J.; Zhang, W.; Stoffelbach, F. o.; Charleux, B. Surfactant-Free RAFT Emulsion Polymerization Using Poly(N,N-dimethylacrylamide) Trithiocarbonate Macromolecular Chain Transfer Agents. *Macromolecules* **2010**, *43*, 6302−6310.

(45) Krevelen, D. W. V.; Nijenhuis, K. T. In *Properties of Polymers: Their Correlation with Chemical Structure*, 3rd ed.; Elsevier: New York, 1990.

(46) In *Polymer Handbook*, 4th ed.; Wiley-Interscience: Toronto, 1999.

(47) Yu, Y.; Zhang, L.; Eisenberg, A. Morphogenic Effect of Solvent on Crew-Cut Aggregates of Apmphiphilic Diblock Copolymers. *Macromolecules* **1998**, *31*, 1144−1154.

(48) Blanazs, A.; Armes, S. P.; Ryan, A. J. Self-Assembled Block Copolymer Aggregates: From Micelles to Vesicles and their Biological Applications. *Macromol. Rapid Commun.* **2009**, *30*, 267−277.

(49) Battaglia, G.; Ryan, A. J. The evolution of vesicles from bulk lamellar gels. *Nat. Mater.* **2005**, *4*, 869−876.

(50) Zehm, D.; Ratcliffe, L. P. D.; Armes, S. P. Synthesis of Diblock Copolymer Nanoparticles via RAFT Alcoholic Dispersion Polymerization: Effect of Block Copolymer Composition, Molecular Weight, Copolymer Concentration, and Solvent Type on the Final Particle Morphology. *Macromolecules* **2013**, *46*, 128−139.

(51) Napper, D. H. In *Polymeric Stabilization of Colloidal Dispersions*; Academic Press: London, 1983.

(52) Roe, R.-J. In *Methods of X-ray and Neutron Scattering in Polymer Science*; Oxford University Press: Oxford, 2000; p 331.

(53) Vogtt, K.; Beaucage, G.; Weaver, M.; Jiang, H. Scattering Function for Branched Wormlike Chains. *Langmuir* **2015**, *31*, 8228−8234.

(54) Pabst, G.; Koschuch, R.; Pozo-Navas, B.; Rappolt, M.; Lohner, K.; Laggner, P. Structural analysis of weakly ordered membrane stacks. *J. Appl. Crystallogr.* **2003**, *36*, 1378−1388.

(55) Alargova, R. G.; Warhadpande, D. S.; Paunov, V. N.; Velev, O. D. Foam Superstabilization by Polymer Microrods. *Langmuir* **2004**, *20*, 10371−10374.

(56) Du, Z. P.; Bilbao-Montoya, M. P.; Binks, B. P.; Dickinson, E.; Ettelaie, R.; Murray, B. S. Outstanding stability of particle-stabilized bubbles. *Langmuir* **2003**, *19*, 3106−3108.

(57) Binks, B. P.; Rodrigues, J. A. Inversion of emulsions stabilized solely by ionizable nanoparticles. *Angew. Chem., Int. Ed.* **2005**, *44*, 441−444.

(58) Binks, B. P.; Murakami, R. Phase inversion of particle-stabilized materials from foams to dry water. *Nat. Mater.* **2006**, *5*, 865−869.

(59) Binks, B. P.; Murakami, R.; Armes, S. P.; Fujii, S.; Schmid, A. pH-responsive aqueous foams stabilized by ionizable latex particles. *Langmuir* **2007**, *23*, 8691−8694.

(60) Bala Subramaniam, A.; Abkarian, M.; Mahadevan, L.; Stone, H. A. Colloid science: Non-spherical bubbles. *Nature* **2005**, *438*, 930−930.

(61) Fujii, S.; Iddon, P. D.; Ryan, A. J.; Armes, S. P. Aqueous Particulate Foams Stabilized Solely with Polymer Latex Particles. *Langmuir* **2006**, *22*, 7512−7520.

(62) Fujii, S.; Ryan, A. J.; Armes, S. P. Long-Range Structural Order, Moiré Patterns, and Iridescence in Latex-Stabilized Foams. *J. Am. Chem. Soc.* **2006**, *128*, 7882−7886.

(63) Dupin, D.; Howse, J. R.; Armes, S. P.; Randall, D. P. Preparation of stable foams using sterically stabilized pH-responsive latexes synthesized by emulsion polymerization. *J. Mater. Chem.* **2008**, *18*, 545−552.

(64) Thompson, K. L.; Fielding, L. A.; Mykhaylyk, O. O.; Lane, J. A.; Derry, M. J.; Armes, S. P. Vermicious thermo-responsive Pickering emulsifiers. *Chemical Science* **2015**, *6*, 4207−4214.

(65) Thompson, K. L.; Mable, C. J.; Cockram, A.; Warren, N. J.; Cunningham, V. J.; Jones, E. R.; Verber, R.; Armes, S. P. Are block copolymer worms more effective Pickering emulsifiers than block copolymer spheres? *Soft Matter* **2014**, *10*, 8615−8626.

(66) Mable, C. J.; Warren, N. J.; Thompson, K. L.; Mykhaylyk, O. O.; Armes, S. P. Framboidal ABC triblock copolymer vesicles: a new class of efficient Pickering emulsifier. *Chemical Science* **2015**, *6*, 6179−6188.

(67) Binks, B. P. Particles as surfactants—similarities and differences. *Curr. Opin. Colloid Interface Sci.* **2002**, *7*, 21−41.

(68) Ciunel, K.; Armélin, M.; Findenegg, G. H.; von Klitzing, R. Evidence of Surface Charge at the Air/Water Interface from Thin-Film Studies on Polyelectrolyte-Coated Substrates. *Langmuir* **2005**, *21*, 4790−4793.

(69) Takahashi, M. ζ Potential of Microbubbles in Aqueous Solutions: Electrical Properties of the Gas−Water Interface. *J. Phys. Chem. B* **2005**, *109*, 21858−21864.

(70) Kettlewell, S. L.; Schmid, A.; Fujii, S.; Dupin, D.; Armes, S. P. Is Latex Surface Charge an Important Parameter for Foam Stabilization? *Langmuir* **2007**, *23*, 11381−11386.